Mat. Res. Soc. Symp. Proc. Vol. 779 © 2003 Materials Research Society W6.6.1

Microdiffraction Experiments and Modeling for Analyzing Multiscale Dislocation Ensembles in Materials

G.E. Ice, R.I. Barabash and J. Pang
Metals & Ceramics Divisions, Oak Ridge National Laboratory, Oak Ridge TN 37831

ABSTRACT

The intensity distribution of Laue diffraction is analyzed as a function of local misorientation. We show how unpaired dislocations alter the white beam Laue patterns for isolated dislocations, for dislocation walls, and for a combination of both. We consider the effect of different statistically and geometrically necessary dislocation densities on the intensity distribution along and perpendicular to the Laue streak. A 3D x-ray crystal microscope is used to analyze the complicated plastic-elastic field in a grain of a Ni polycrystalline sample during in-situ uniaxial pulling. A change of dislocation activity with depth is demonstrated. The dislocation slip systems and their densities are determined at various depths. The model parameters are used to simulate the whole Laue pattern including details about the contours for specific Laue spots; good agreement is found between simulated and experimental contours.

INTRODUCTION

The recent developments of strain gradient plasticity represent an effort to bridge the gap between classical plasticity and dislocation theory[1-4]. Plastic strain gradients appear either because of the geometry of loading or because the material is plastically inhomogeneous. Several length scales are introduced in the framework of strain gradient plasticity. Considering different models of geometrically necessary dislocations, GNDs, Gao[3] *et al*. related effective strain gradient η to the density of GNDs, n^+. Polychromatic x-ray microdiffraction offers a fundamentally new approach to the study of mesoscale dynamics in single crystals and polycrystalline materials[5,6]. With white-beam microdiffraction it is possible to quantitatively analyze a sample at different structure levels. In particular, it is now possible to analyze details of structure corresponding to nano (cells) - and mesoscopic (fragments) levels. Different slip systems cause distinctly different streaking in their Laue patterns. Examination of streaked patterns enables the detection of statistically stored dislocations and GNDs, and the quantitative determination of dislocation patterning parameters. We use a multiscale hierarchical framework similar to a cell-wall model[7-8], o extend the dislocation/disclination description for the length scales introduced in strain gradient plasticity theory. We show that diffraction experiments give natural criteria for the aforementioned length scales.

EXPERIMENTAL DETAILS

The 3D x-ray crystal microscope uses a modified Laue diffraction method based on polychromatic radiation[5,6]. This approach allows for true 3D mapping of crystalline phase, orientation, elastic strain and plastic deformation with unprecedented spatial resolution. As the polychromatic beam penetrates the sample, it produces a Laue pattern in each subgrain that it intercepts. The overlapping Laue patterns are detected by an x-ray sensitive CCD positioned at

90° to the incident beam. The origin of each Laue pattern can be decoded with a wire that scans through the diffracted beams. This decoding technique is called differential aperture microscopy. In a typical experiment, the sample is mounted on a precision 3-axis rectilinear sample stage with 25 nm bi-directional repeatability. A region of interest is identified using an optical microscope and the polychromatic x-ray beam is focused onto the sample. Overlapping Laue images from grains probed by the beam, are recorded by the CCD. The number of grains or subgrains illuminated by the penetrating x-ray beam is identified, and the orientation of each subgrain is precisely determined by an automated indexing program. Details on the experimental setting and data collection can be found elsewhere[5,6]. Data collection has been carried out using microbeam Laue diffraction on beamline ID-34E at the APS. In this experiment, rotations of five neighbouring grains in a polycrystalline Ni tensile sample was determined at 0, 10 and 15% mesoscopic plastic strain (Fig.1). Dimensions of the beam were 0.46 by 0.55 micron with a penetration depth of ~ 30 micron. Rotation of grains at depth can be resolved to a resolution of ~1 micron using the differential aperture microscopy[6].

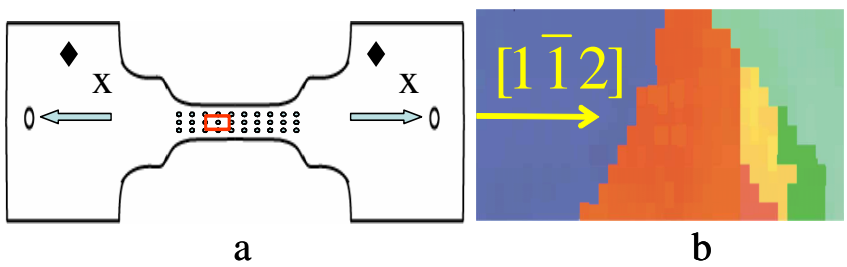

Figure. 1 Experimental setup for in situ uniaxial pulling (a) and marked square region with five neighbouring grains in a polycrystalline Ni tensile sample (b).

RESULTS AND DISCUSSION

In traditional white-beam Laue diffraction, a continuum spectrum is diffracted by a single crystal (or single grain). The crystal scatters the beam into a characteristic Laue pattern that depends on the crystal space lattice, its orientation and the incident-beam energy distribution. The incident beam and scattered beam directions defines a line in reciprocal space. The position along this line is determined by the wavelength of the scattered radiation. For example reciprocal lattice points (00h), (002h), (003h), (004h) *etc* are scattered towards the same pixel on a detector but lie at different positions radially in reciprocal space. To analyze the white beam intensity distribution from a deformed grain, we introduce *unit* vectors in each direction of scattering $\hat{\mathbf{k}} = \mathbf{k}/|\mathbf{k}|$. We define a special misorientation vector ***m*** near a Bragg reflection[9,10] $\mathbf{m} = \hat{\mathbf{k}} - \hat{\mathbf{k}}_{hkl}$. The misorientation vector **m** gives the difference between the unit vectors parallel to a Bragg reflection (*h k l*), $\hat{\mathbf{k}}_{hkl}$, and an arbitrary direction in its vicinity, $\hat{\mathbf{k}}$.

We have analyzed the diffracted Laue images for patterning at several structural levels involved during plastic deformation. We start with diffraction for the first structural level: individual randomly spaced statistically stored dislocations and GNDs. During deformation dislocation motion and the strong interaction between dislocations collect individual dislocations to create a correlated dislocation arrangement with dislocation walls. Some fraction of the dislocations may remain randomly distributed, and the rest will form various correlated dislocations and more organised disclination arrangements. Neighbouring cells are usually separated by the "so called" incidental dislocation boundaries[10] (IDBs). The next structural level involves fragments. Fragments contain cells with approximately the same crystallographic

orientation. Geometrically necessary boundaries (GNBs) separate two fragments. For crystals with unpaired tilt dislocation walls (GNBs or IDBs), X-ray diffraction Laue spots are broadened in proportion to the number of excess dislocations inside the wall and to the total number of unpaired walls.

In the mechanism-based strain-gradient plasticity (MSG) framework, plastic deformation is described[1-4] by a strain gradient tensor of the third rank η_{lmk} with effective strain gradient $\eta = \sqrt{c_1\eta_{iik}\eta_{jjk} + c_2\eta_{ijk}\eta_{ijk} + c_3\eta_{ijk}\eta_{kji}}$ and constants c_1,c_2,c_3. The plain-strain bending of a crystal of curvature K usually is modeled by a network of randomly distributed GNDs with the density n^+ and Burgers vector **b** (Fig.2a). The curvature K= n^+b coincides with the above effective strain gradient η. This enables us to write η in terms of the density of GNDs, η=n^+b. The average distance between randomly distributed GNDs at yielding, L_s, is related to the "material length *l*" in the MSG theory[3,4]. We write the strain gradient tensor η_{lmk} in terms of the anti-symmetric Levi-Civita tensor of third rank ε_{ilm} and a dislocation density tensor of second rank ρ_{ik}:

$$\varepsilon_{ilm}\eta_{lmk} = -\rho_{ik} = -\tau_i b_k \delta(r), \quad \eta_{lmk} = \partial^2 u_k / \partial x_l \partial x_m . \qquad (1)$$

Here u_k, the *k*-th component of the displacement field **u** for any unit cell, is due to all dislocations in the crystal. We calculate the total displacement of the *i*-th cell $\boldsymbol{u}_i$ from the equilibrium positions $\mathbf{R}_i^0$ corresponding to the undeformed crystal using continuum elastic theory. This displacement is due to all dislocations and is defined using random numbers c_t by the equation[9,10] :

$$\mathbf{u}_i = \sum_t c_t \mathbf{u}_{it} ; \qquad c_t = \begin{cases} 1, (+) \\ 0, (-) \end{cases} \qquad (2)$$

If there is a dislocation at position *t*, $c_t = 1$, and for positions without dislocations $c_t = 0$. The Cartesian reference frame is set such that the x_1 axis coincides with the direction of Burgers vector $\boldsymbol{b}$ and x_3 coincides with the direction of dislocation lines of the dislocation net. With this coordinate system the crystal will be bent in the plane x_1x_3 due to the net of GNDs. In this Cartesiain reference frame the only nonzero components of the dislocation density tensor is ρ_{31} resulting in the nonzero components of the strain gradient tensor: $\eta_{112} = -K$ and $\eta_{211} = K$, with effective strain gradient $\eta = K = n^+b$.

Plain-strain bending can be modelled by walls of GNDs as well as by randomly distributed GNDs (Fig.2b). These walls are responsible for the next structural level and are related to the second intrinsic length scale. Consider the structure with geometrically necessary randomly distributed tilt dislocation boundaries. We assume pure tilt boundaries formed by equidistant edge GNDs (so called "thin walls") with mean distance between the dislocation lines within the wall equals *h* (Fig.2b). These boundaries do not produce long-range elastic strain but generate subgrain rotations. Each wall provides a rotation between two neighboring mosaic blocks with rotation angle Θ. To characterize this model quantitatively we define the average distance *D* between GNBs and write the number of GNBs per unit length as $1/D$. This distance corresponds to the second intrinsic length scale in the MSG approach. The total density of GNDs grouped in

the GNBs is denoted by $n^{+} = 1/Dh$. The effective strain gradient in this model can be written as $\eta = \Theta / D$.

Dislocations change the diffraction conditions and enlarge the region of high intensity around each Bragg position. The intensity distribution *I (q)* of x-ray (or neutron) scattering due to defects can be computed from the expression:

$$I(\mathbf{q}) = f^{2} \sum_{i,j} e^{i\mathbf{q}\bullet\mathbf{R}_{ij}} e^{-T} \qquad T = nS \sum_{t} 1 - e^{\left(i\mathbf{Q}\bullet(\mathbf{u}_{it} - \mathbf{u}_{jt}\right)} \tag{3}$$

Here f_i is the scattering factor from an individual atom *i*, with relaxed co-ordinates $R_i = \mathbf{R}_i^0 + \mathbf{u}_i$ due to the presence of defects; *S* is the area of one dislocation in a transverse plane; *n* is the total dislocation density, and *nS* is a dimensionless quantity that indicates the fraction of lattice sites covered with dislocations. Following the approach described in the reference[10] the difference between displacements of two scattering lattice cells i and j can be written

$$\mathbf{u}_{it} - \mathbf{u}_{jt} = (\mathbf{R}_{ij}\nabla)\mathbf{u}_{it} + \frac{1}{2}(\mathbf{R}_{ij}\nabla)^{2}\mathbf{u}_{it}, \tag{4}$$

where $\nabla \equiv \nabla_{R_i}$. The correlation function T differs for different dislocation arrangements and depends on the density of GNDs and effective strain gradient parameter[10]. In general for an arbitrary distribution of statistically stored dislocations and GNDs T has both real and imaginary parts, $T = T_2 + iT_1$, where

$$T_1 = \sum_{ti} c_i (\mathbf{R}_{ij}\nabla)(\mathbf{G}_{hkl}\mathbf{u}_{it}); \qquad T_2 = -\sum c_i \left[1 - \cos\left[(\mathbf{R}_{ij}\nabla)(\mathbf{G}_{hkl}\mathbf{u}_{it})\right]\right]. \tag{5}$$

With substitution of Eq. 2 and 4 into 5, we find that for unpaired dislocation walls density in system λ of n_{λ}^{+}

$$T_1 = -iC_1 \sum_{\lambda} n_{\lambda}^{+} (\mathbf{R_i} \bullet \mathbf{b}_{\lambda})\left(\left[\mathbf{Q} * \mathbf{R}_{ij}\right]\boldsymbol{\tau}_{\lambda}\right); \qquad T_2 = C_2 (Qb)^2 \ln L \sum_{\lambda} n_{\lambda}\varphi_{\lambda}. \tag{6}$$

Here C_1, C_2 are the orientation and radial contrast factors, λ is the number of the activated

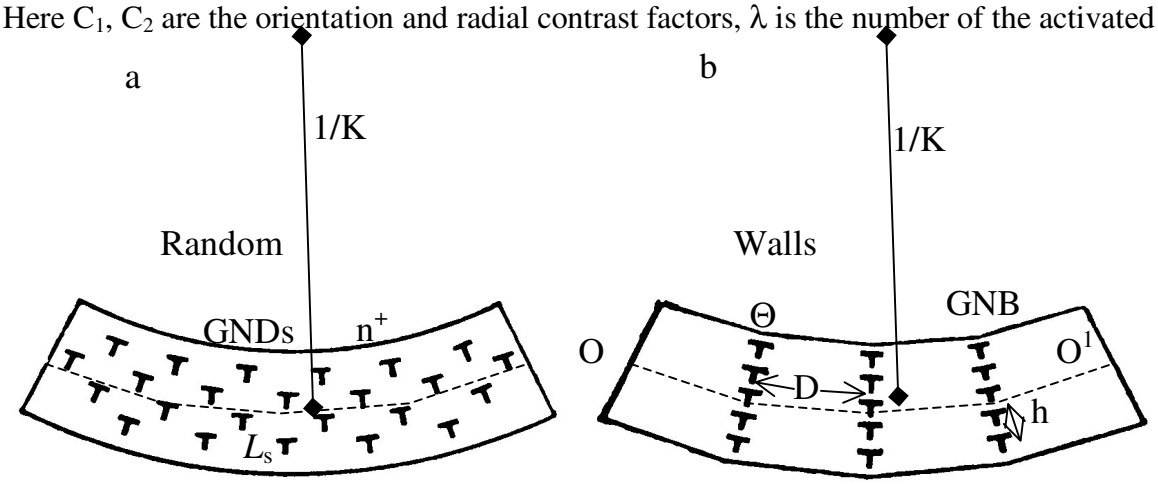

Figure. 2 Scheme of the randomly distributed geometrically necessary dislocations (a) and their polygonization into cell-walls (b) corresponding to the plain strain bending of a crystal in the x_1x_2 plane with curvature K relatively neutral plane OO^1; $K = n^{+}b$ for random distribution (a) and $K = \Theta / D$ for dislocation groupings in the walls (b).

dislocation slip system, L is the size of the subgrain (or the cut-off radius), and φ_λ is the orientation factor for each dislocation system. The first term T_1 is imaginary, linear with respect to the density of unpaired dislocations n^+ and goes to zero when $n^+ = 0$. The real part of the correlation function T_2 is independent of whether dislocations are paired or unpaired. From the structure of this equation it follows that dislocations parallel to the diffraction vector do not contribute to the function T_1 and do not influence the intensity of scattering (contrast factor C_1 for these dislocations is zero). T_2 describes the influence of mean distortions due to randomly distributed individual GNDs.

For an equal number of random "+**b**" and "-**b**" dislocations the broadening of the diffuse scattering is induced by random local fluctuations in the unit cell orientations and d spacing that tend to cancel out over long length scales. Due to the character of the displacement field around edge GNDs, displacements occur only in planes perpendicular to the direction of dislocation lines $\boldsymbol{\tau}$. As a result, coherence is not changed along the direction $\boldsymbol{\tau}$, and the diffracted intensity in this direction is the same as for crystals without dislocations. Perpendicular to $\boldsymbol{\tau}$, the intensity distribution is roughly symmetric with a characteristic full width at half maximum (FWHM) dependent on the total dislocation density n: $FWHM \propto \sqrt{n}$. For unpaired dislocations or dislocation walls the Laue intensity distribution relates the distortion tensor, ω_{ij}, due to GNDs, n^+, to the unpaired dislocation density and system (direction $\boldsymbol{\tau}$, and Burgers vector **b**).

Near a Laue reflection, we can define[11] two natural axes ξ and ν in the plane perpendicular to the momentum transfer unit vector **g**. With this co-ordinate system, the diffuse scattering is strongly elongated in the ξ direction, and the full width at half maximum in the ξ direction $FWHM_\xi$ for randomly distributed GNDs depends on their density, n^+, mutual orientation between the active dislocation system, the momentum transfer unit vector **g**, and the length of the coherently scattering region *L*. In the narrow direction, ν, the $FWHM_\nu$ depends on the average distance between statistically stored dislocations L_s and on the mutual orientation between $\boldsymbol{\tau}$ to **g**. For groupings of GNDs in the walls the $FWHM_\xi$ depends on the average distance *D* between GNBs, their mutual orientation to the momentum transfer **G**, the type of GNB (tilt or twist), and the incident x-ray beam direction.

$$FWHM_\xi \propto \eta L f_\xi(\hat{\tau} \bullet \hat{G}_{hkl}); \qquad FWHM_\nu \propto b L_s^{-1} f_\nu(\hat{\tau} \bullet \hat{G}_{hkl}) \qquad (6)$$

Here $f_\xi(\hat{\tau} \bullet \hat{G}_{hkl})$ and $f_\nu(\hat{\tau} \bullet \hat{G}_{hkl})$ are contrast factors along and perpendicular to the streak. The predominant slip systems and direction of the strain gradient can be identified because of their distinctly different contributions to streaking of the Laue patterns. We emphasize that in white beam diffraction the FWHM is a function of misorientation vector ***m*** between unit vectors (rather than reciprocal space momentum transfer vector).

The microbeam-Laue technique was applied to a complicated dislocation structure arising from the *in situ* uniaxial pulling in a Ni polycrystalline sample. The microbeam-Laue diffraction reveals pronounced streaking of Laue images after 15% of strain. The plastic response of the material in each grain can be described by formation of GNDs in the material to relax the stress field induced during pulling. In FCC crystals, typical edge dislocation lines are parallel to the directions of <112> with Burgers vectors being parallel to the directions <110> and corresponding glide planes {111}. Laue images were taken at different depth of a grain labeled A in the Ni polycrystalline sample. The orientation of the grain surface normal after deformation was almost parallel to $[\bar{2}33]$ with loading direction approximately in $[1\bar{1}2]$ direction.

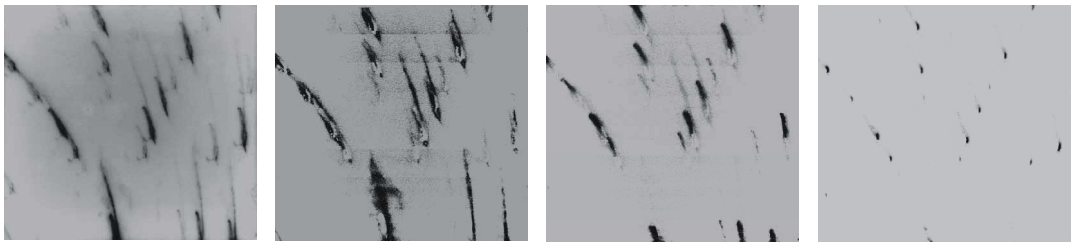

a b c d

Figure. 3 Experimental Laue images from the grain A of a polycrystalline Ni sample after 15% of strain: a)Laue pattern from the total depth of 30μm (a) and depth resolved patterns obtained from the depth of 5μm (b); 15μm (c); 28μm (d).

Experimental Laue patterns from a depth of 30 μm and depth resolved images with 1μm resolution obtained with differential aperture microscopy[6] are shown in Fig.3. Distinct streaking of the Laue spots is observed up to 25μm below the sample surface. The total Laue pattern obtained from 30μm consists of two sets of streaks (Fig.3a). It is an indication that at least two regions with different slip systems and different strain gradient direction are present in the irradiated volume. Differential aperture microscopy demonstrated that in the near-surface region only one set of very-long streaks is present (Fig.3b).

To understand the shape of the experimental Laue images and to check the sensitivity of the Laue image to different possible orientations of GNDs, we have simulated Laue patterns with different GND slip systems with the same density of GNDs. Some of them are shown at the Fig.4. Simulations were performed for cell-wall structure of GNDs. Geometrically necessary boundaries (GNBs) were formed by dislocations with Burgers vector **b=** ||[110] and dislocation lines in $[1\bar{1}\bar{2}]$ and $[1\bar{1}2]$ directions.

Using the aforementioned analysis we determined the direction of the activated slip system in the near-surface region and simulated Laue pattern corresponding to the best fit slip system parameters (Fig.5). At 15 μm depth we observe a change in the slip system direction. At a depth of 25μm the Laue pattern consists of relatively well shaped spots. However comparison of the sample orientation matrix at increasing depth shows that it continues to rotate. Our analysis of the orientation of the activated dislocation slip systems shows that the slip systems with dislocation lines inclined approximately 45 degrees to the loading direction are activated first.

While the general features of uniaxial plastic deformation have been considered in the literature[11-15], a direct quantitative analysis of the geometrically necessary dislocations formation within several length scales within each grain and comparison with strain-gradient plasticity parameters is presented here for the first time.

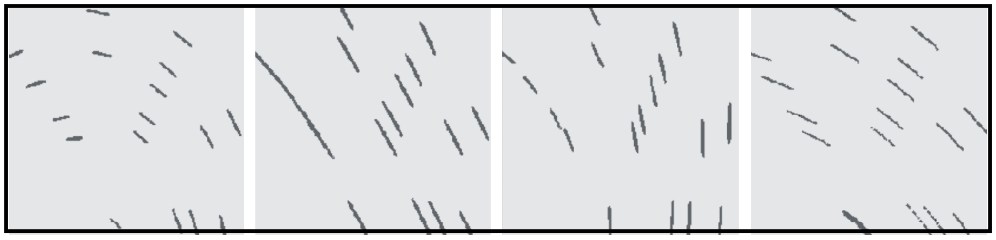

a b c d

Figure.4 Laue patterns simulated with different orientation of GNDs of the same density, (orientation of the crystal is chosen to coincide with Fig.3d):a) b [0-11] ξ [-211];b) b [1-10] ξ [112]; c)b [110] ξ [1-12] +ξ [1-1-2];d) b [0-11] ξ [211].

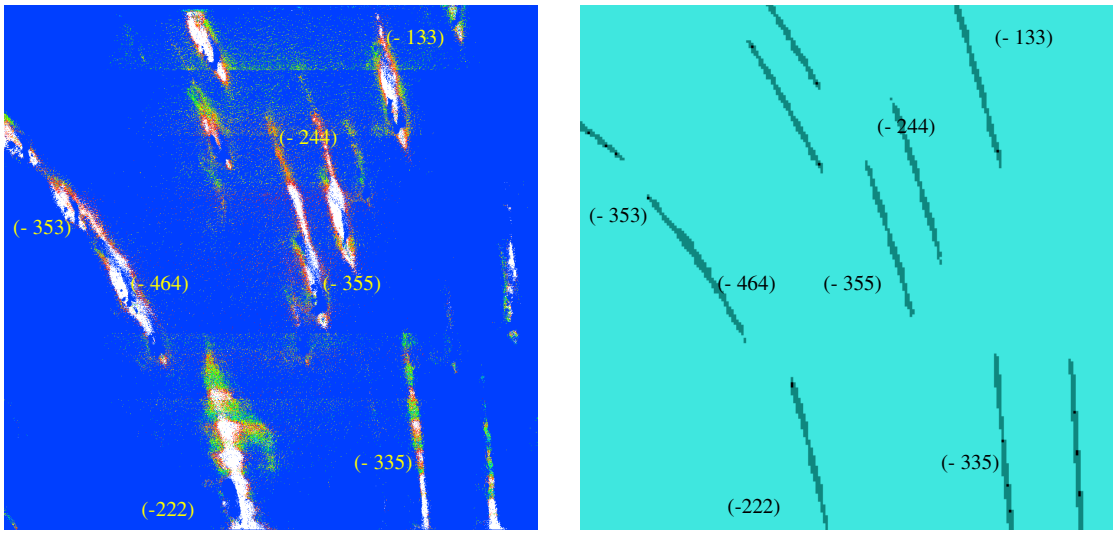

Figure.5 Experimental (left) and simulated (right) Laue pattern at the depth 5μm beneath the surface.

ACKNOWLEDGEMENT

Work sponsored by the Division of Materials Sciences through the Oak Ridge National Laboratory. Oak Ridge National Laboratory (ORNL) is operated by UT-Battelle, LLC, for the U.S. Department of Energy under contract DE-AC05-00OR22725. Work in part on Unicat beamline 34-ID at the Advanced Photon Source (APS), which is supported by the Univ of Illinois at Urbana-Champaign, Materials Research Laboratory (U.S. DOE, the State of Illinois-IBHE-HECA, and the NSF), and by the Oak Ridge National Laboratory (U.S. DOE under contract with UT-Battelle LLC). The APS is supported by the U.S. DOE, Basic Energy Sciences, Office of Science under contract No. W-31-109-ENG-38.

REFERENCES

1. Fleck N., Muller G., Ashby M., Hutchinson J., Acta Metall. Mater., **42**, 2, 475, (1994).
2. Begley M.R., Hutchinson J.W., J. Mech. Phys. Solids, **46**, 2049, (1998).
3. Gao, H., Huang, Y., Nix, W.D. and Hutchinson, J.W., J. Mech. Phys. Solids, **47**, 1239, (1999)
4. Huang Y., Gao H., Nix W., Hutchinson J., J. Mech. Phys. Solids, **47**, 1239, (2000).
5. Ice G.E. and Larson B.C., Adv. Eng. Mater., **2**, 10, 643, (2002).
6. Larson B.C., Wenge Yang, G.E.Ice, J.D.Budai, J.Z.Tischler, Nature, **415**, 887, (2002).
7. Mughrabi H., Ungar T., Kienle W., Wilkens M. Phil. Mag. **A53**:793, (1986).
8. D. Hughes and N. Hansen, Acta Mater. **48**, 2985-3004, (2000).
9. R. Barabash, G.E. Ice, B.C. Larson, G.M. Pharr, K.-S. Chung, W. Yang, Appl. Phys. Lett., **79**, 749, (2001).
10. R. Barabash, G.E. Ice, F.Walker, J.Appl.Physics, **93**, 3, 1457-1464 (2003).
11. Hecker H., Thiele E., Holste C., Acta Mater. **50**, 2357,(2002).
12. Schwink C. Scripta Metall **27**, 963, (1992).
13 Huang, X. and Hansen, N., Scripta Mater. **37**(1),1-7, (1997)
14. Winther, G., et al., in "Textures of Materials", Pts 1 and 2. 2002. p. 287-292.
15. Tatschl, A. and O. Kolednik, Mater. Sci. Engineering, **A 342,** 1-2, 152, (2003).